PhD thesis

Functional protein dynamics studies by fluorescence and ultrafast spectroscopy

Katalin Kilián Balázsné Raics

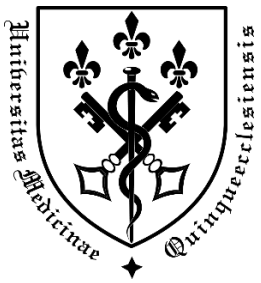

University of Pécs
Medical School
Department of Biophysics

Interdisciplinary Medical Sciences Doctoral School (D93)
Leader of the doctoral school: Prof. Dr. Balázs Sümegi†, Ifj. Prof. Dr. Ferenc Gallyas
Program: Investigating functional protein dynamics using biophysical methods (B-130)
Leader of the program: Prof. Dr. Miklós Nyitrai
Supervisor: Dr. András Lukács, Dr. Emőke Bódis

Pécs, 2024

Introduction

Photoactive flavoproteins

Photoactive flavoproteins are plant blue-light-sensing photoreceptors that bind riboflavin derivatives; they respond to illumination via flavin. A fraction of flavin-containing proteins are photoactive; they are classified into three groups according to how they respond to light: photolyases/cryptochromes, Light Oxygen Voltage (LOV) proteins and Blue Light Sensing Using FAD (BLUF) domain proteins. While in the best-known photoreceptor families (e.g. rhodopsin, phytochrome, and xanthophin) light sensing occurs following chromophore cis-trans isomerization, in the case of flavoproteins the primary step following illumination may be electron/proton transfer, cysteine adduct formation, or remodelling of the hydrogen bond system. While electron transfer plays a key role in the function of cryptochromes and photolyases[6-12], it is clear that BLUF domain proteins become functional after rearrangement of the hydrogen bond system around flavin in response to light[13-15]. However, the mechanism underlying the structural change is not always completely clear, as the presence of light-induced electron transfer (proton-coupled electron transfer) processes has been demonstrated in about half of the known BLUF domain proteins, either in parallel with or preceding the remodelling of the hydrogen bond system.

Many blue-light-sensing photoreceptors use flavin as a chromophore, where light absorption is localised in the flavin (isoalloxazine) ring. Flavins, in neutral or anionic form, can switch between three different redox states by electron uptake or loss: the fully oxidized (FADox), the one-electron reduced or semiquinone ($FADH^{\bullet}$) form, and the hydroquinone ($FADH_2$), the two-electron fully reduced form. Two redox pairs, the oxidized flavin/anionic semiquinone (FAD_{OX} and $FAD^{\bullet-}$) and the neutral semiquinone/anionic hydroquinone ($FADH^{\bullet}$ and $FADH^{-}$), are frequently involved in electron transfer processes. The spectroscopic properties of the different oxidized states of FAD allow the monitoring of reactions involving changes in oxidation state by UV-visible absorption and fluorescence spectroscopy. Each redox state of FAD has a different absorption spectrum, so that the change of oxidation state can be easily observed.

Oxidized flavins have an absorption maximum at around 450 nm and fluorescence peak at ~515-520 nm. The change in redox potential (from about -0.3 V to about +1.9 V) upon photoexcitation is a fundamental parameter for understanding flavin photochemistry, indicating that flavins are much stronger oxidants in the excited state than in the ground state.

Within proteins and even in solution, flavins act as electron acceptors, i.e. in the excited state they accept electrons from their environment (nearby molecules).

The BLUF domain proteins

The BLUF domain is a modular unit found in many blue light-sensing proteins; one tenth of bacteria contains BLUF proteins. Members of the flavin family of blue light-sensing proteins (BLUF) may have functions such as regulating enzyme activity, phototaxis, photophobic response, or gene expression[15,20-24]. For all BLUF domains, a 10-15 nm shift of the flavin absorption peak around 450 nm can be observed upon illumination due to a rearrangement of the hydrogen bond system around the FAD. This is considered to be a marker of their photoactivation ability. All BLUF domains contain a tyrosine close to the flavin, glutamine and, with one exception, a tryptophan.

Structure and photophysics of the OaPAC protein

Photoactivated adenylate cyclases (PACs) are light-activated enzymes that combine blue light sensing with the ability to convert ATP to cAMP and pyrophosphate (PPi) in a light-dependent manner. OaPAC ('Oa' signals that it originates from the photosynthetic cyanobacterium *Oscillatoria acuminata*), a member of the photoactivated adenylate cyclase (PAC) family, is a homodimer consisting of an N-terminal BLUF domain and a C-terminal type III adenylyl cyclase (AC) domain[27,28].

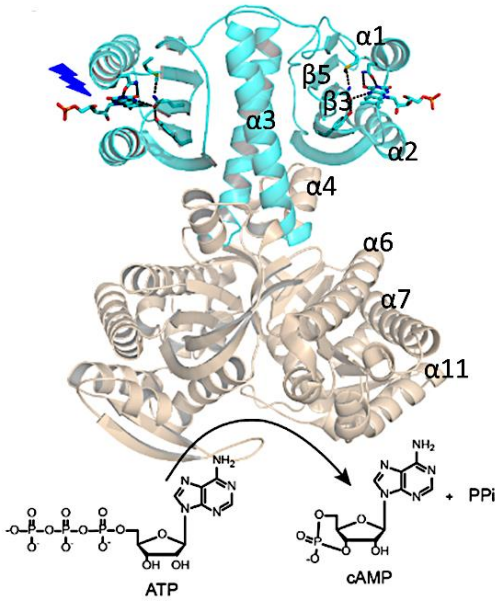

Figure 1. *Structure of OaPAC (PDB 5X4T) with the light-sensing BLUF domain and the AC domain, that is responsible for ATP-cAMP conversion (Lukács et al 2022.)*

Photoactivation is controlled by the BLUF domain at the N-terminal end of the enzyme. The catalytic domain is adenylate cyclase (AC) which contains an ATP-binding site. The BLUF unit responds to blue light through flavin and thereby regulates the activity of the attached enzyme. Thus, we can distinguish and name the dark (inactive) and light (active) states of the protein. The structural differences between the dark and light states are very small when examined in the case of crystallised proteins, but they are coordinated shifts that induce up to 20-fold increase in enzyme activity tens of angstroms away from the chromophore.

The BLUF domain-coupled adenylate cyclase converts ATP into cAMP, a molecule that acts as a secondary messenger in various signalling processes, regulating a myriad of cellular functions. Since OaPAC shows the lowest activity in the dark of all PAC proteins described so far, blue light immediately triggers cAMP production, i.e. the rate of ATP conversion to cAMP increases abruptly. The possibility of fine-tuning the control of cAMP production by light thus makes OaPAC a model system of high importance in optogenetic research.

During the conversion of ATP to cAMP the enzyme forms a cyclic phosphodiester bond between the α-phosphate group of ATP and the OH group of the 3' C atom in ribose. This leads to release of pyrophosphate. In the OaPAC protein, the light-excitation-activated adenylate cyclase abruptly increases the rate of conversion of ATP to cAMP, leading to an increase in the intracellular cAMP level. The AC activity of OaPAC can be increased by light up to 20-fold compared to baseline levels in the dark. (The optimal optogenetic device should be "quiet" in the dark, but highly responsive to light.)

The changes in OaPAC in response to blue light are due to interactions between the isoalloxazine ring of FMN and nearby amino acids on the β3 fold (Figure 2). Blue-light excitation of the BLUF domain of OaPAC results in a proton-coupled electron transfer process, where the primary electron and proton donor is the tyrosine near flavin (Y6). Electron transfer to flavin is accompanied by a rearrangement of the hydrogen bond network. The induced structural changes presumably extend towards the AC domain, allowing the conversion of ATP to cAMP.

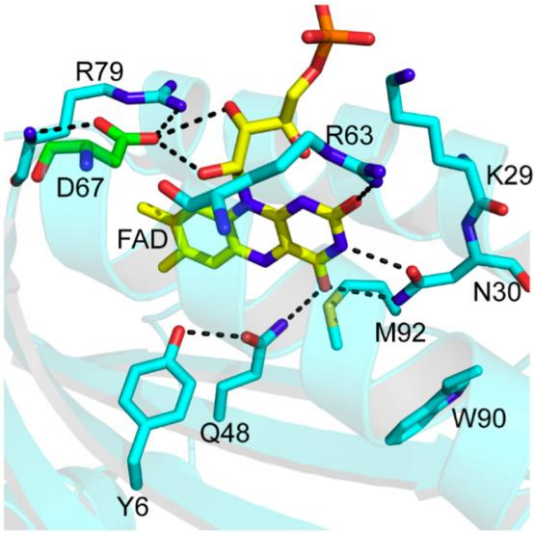

Figure 2. *Environment of the isoalloxazine ring in OaPAC: residues Y6, D67 and W90, which play a key role in the photophysics of OaPAC (PDB: 4yus[22]).*

The primary photochemistry of OaPAC is therefore determined by a proton coupled electron transfer (PCET)[33] process (Figure 3). When a blue light photon is absorbed, an electron is transferred from the nearby tyrosine (Y6) to flavin - the electron transfer step results in an anionic ($FAD^{\bullet -}$) or neutral flavin radical ($FADH^{\bullet}$) depending on the flavin environment - and

simultaneously a proton is transferred from Y6 to the neighbouring glutamine (Q48). This proton is subsequently transferred to flavin, stabilizing the neutral semiquinone state of flavin (the flavin radical is protonated to form the half-quinone form). During the PCET process, the Q48 glutamine is turned or tautomerized, which is presumably important in transmitting the signal to the C-terminal part of the protein where the ATP → cAMP conversion takes place.

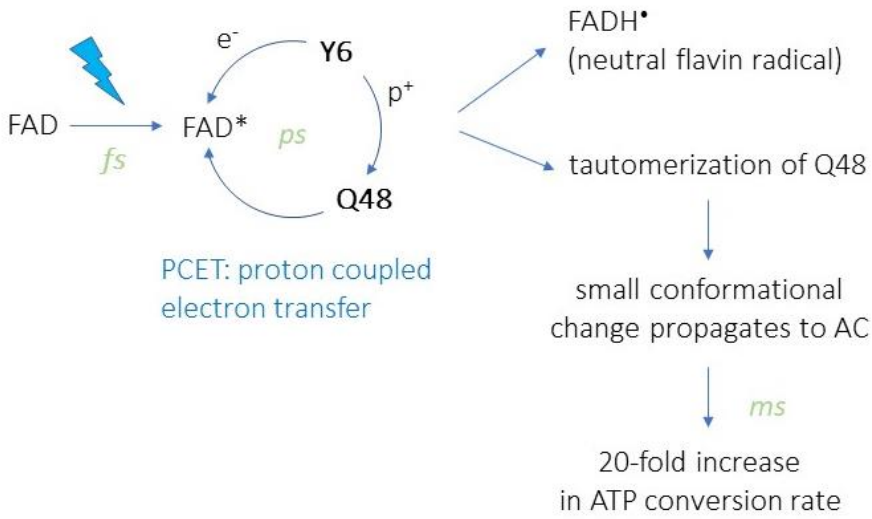

Figure 3. *Steps following blue light absorption in the OaPAC protein until ATP-cAMP conversion occurs in the AC domain.*

The D67N mutant of OaPAC

Based on adiabatic quantum mechanics/molecular mechanics simulations performed on another protein containing a BLUF domain with significant homology to the BLUF domain of OaPAC, Slr1694 (also known as PixD), the authors suggested[40] that replacing the negatively charged residue D69 with a neutral or positively charged residue would have a major impact on the electron transfer process. Since the replacement of the negatively charged residue at position 69 with a neutral residue in PixD is predicted to enhance the electron transfer process, we were interested in the effect that an analogous mutation in OaPAC (replacement of the negatively charged aspartic acid at position 67 with a neutral asparagine (D67N)) might have on the functional dynamics of the protein. Since model calculations suggest that disruption of H-bonds affects PCET and the enzymatic properties of the protein, the D67N mutation appears to be an excellent candidate for producing more efficient optogenetic systems, despite the distance of D67 from Y6.

Objective

Our objective was **to increase the enzyme activity of the photoactivated adenylyl cyclase OaPAC** from the photosynthetic cyanobacterium *Oscillatoria acuminata* by optimizing the electron transfer process in the BLUF domain through mutagenesis. The mutation involving a residue near the flavin chromophore binding site (an aspartic acid was replaced by asparagine in this region) is justified by previous QM calculations, which suggest that it affects the photochemical properties of the system in a way that may be useful for optogenetic purposes.

We were curious to see how the mutation affects the electron transfer process and the ATP-cAMP conversion. To study the above processes we aimed at **characterising the photophysical properties of the OaPAC D67N mutant** by transient absorption and time-dependent fluorescence spectroscopy, complemented by enzyme activity studies as well as fluorescence anisotropy and differential calorimetry methods.

Our aim was to experimentally study the nature of the electron transfer and the active state lifetime of the D67N mutant in the first step of the reaction and to understand the role of the electron transfer in the function of OaPAC.

Materials and methods

Ultrafast spectroscopy methods

To follow absorption spectral changes on a very short, picosecond to femtosecond time scale and to characterise the electron transfer processes of flavoproteins through this spectral magnification, we used visible transient absorption (TA) and Kerr-gated fluorescence spectroscopy techniques, both based on the pump-probe principle. The redox states of the flavin chromophore, which depend on the protein environment and photochemistry, have well-differentiated absorption spectra and can be well measured. In the TA technique, the sample is excited by a relatively high intensity laser pulse (pump). To monitor the effect over time, a series of much lower energy probe pulses illuminate the sample at fixed time intervals: this way the excited state absorption can be studied. The temporal resolution is determined by the length of the probe pulse, which in our system is 100 fs; thus, the instrument is suitable for the investigation of processes in the range 100 fs - 100 ps. The applied pump beam is a 400 nm beam of light generated by a frequency-doubling BBO (beta barium borate) crystal, and the probe beam is a broad-spectrum white light continuum in the 380-700 nm range generated from the 800 nm pulsed laser using a CaF_2 plate.

The light source was a Spectra-Physics Mai Tai type Ti:Sa laser oscillator (100 fs pulse length, 100 MHz repetition rate, 1.5 W average power, 1 nJ energy) pumped by a Nd:YLF laser. This illuminated the Ti:Sa medium of the laser amplifier (Spectra-Physics Spitfire Ace), which was pumped by another Nd:YLF laser (Spectra Physics Empower; Intracavity-Doubled, Diode-

Pumped Nd:YLF Laser Systems). The output beam had a wavelength tunable between 710 and 990 nm, a pulse length of 100 fs at 800 nm, a repetition frequency adjustable in the range 1-5 kHz, and an energy of 1 mJ after amplification. One of the split laser beams passed through the BBO crystal at a wavelength of 400 nm to excite the sample regularly, while the other beam passed through the CaF_2 plate after the delay unit and illuminated the sample as a white light test pulse. The beams overlaped in the sample, where the effect produced by the 400 nm pump pulse was "probed" by the white light delayed in time steps.

The absorption spectra were recorded by an Andor Newton CCD operating at -80°C. The absorption data matrices were calculated by a custom program written in NI LabVIEW software. The resulting data matrix was analysed using Glotaran[2] software.

In the Kerr-gated fluorescence spectroscopy technique, the probe pulse does not meet the pump in the sample, but in the so-called Kerr medium. Its role is to open a suitable time window in the fluorescence process in the sample, after which the intensity and wavelength of the emitted photons can be measured. The high intensity of the probe pulse causes the plane of polarisation of the in-plane polarised (in this case fluorescent) light passing through the birefringent Kerr medium to be reversed. The fluorescent light coming out of the sample becomes plane-polarized after passing through a polarizer. A second polarizer is set perpendicular to this, so that light can only pass through the second polarization filter if the Kerr effect causes the high-energy probe pulse to open the Kerr medium. The plane of the fluorescent light is then rotated, so a fraction of the light passes through. By controlling the exact time of transmission and by measuring the intensity of the fluorescence, the decay process can be reconstructed.

The homemade setup allowed us to record fluorescence spectra with a time resolution up to 100 fs and on a time scale of up to ns. The excitation pulse at 390 nm was obtained by frequency doubling of a part of the 780 nm laser pulse using a BBO crystal operating at 1 kHz. The remaining 780 nm beam passed through a delay stage and focused into the Kerr medium, where it overlapped spatially with the fluorescence of the sample. The Kerr medium used was CS_2. The sample was flowed through the optical cell with a 1 mm path length using a peristaltic pump. Transient fluorescence spectra were measured for each sample with a time delay up to 1500 ps. Global analysis of the time and spectral resolution data series was performed using Glotaran.

Indirect measurement of cAMP – Pyrophosphate assay

To quantify the ATP-cAMP conversion rate in the wild-type OaPAC and the D67N mutant, EnzChek® pyrophosphate assay was used. The procedure is based on a pyrophosphate-dependent increase in the light absorption of 2-amino-6-mercapto-7-methylpurine at 360 nm.

The ATPase activity of OaPAC wild-type and D67N mutant ATPases detected at 1 M concentration was performed in the dark and under continuous 473 nm, 9 mW laser illumination

in the presence of 500 M ATP. Reaction buffer (20x: 10 mL 1.0 M Tris-HCl, 20 mM $MgCl_2$, pH 7.5, 2 mM Na azide), IP (3 μM/ml), 1 mM MESG (20 μM), PNP (100 μM/ml) were added to the protein, incubated for 1-2 min at 22°C, and the reaction was started by the addition of ATP. The reaction rate (in μM/s) of the purine-based molecule (2-amino-6-mercapto-7-methylpurine), which is the same as the reaction rate of ATP-derived pyrophosphate, was determined from the slope of the absorbance change at 360 nm.

To determine the Michaelis-Menten constant, the assay was performed on 1 μM wild-type and D67N mutant in the presence of 0-500 M ATP concentrations at nine different concentration values. The resulting rate constants were plotted as a function of ATP concentration. By fitting the Michaelis-Menten saturation curve of the enzyme reaction, the maximum reaction rate (v_{max}) and the corresponding K_M, which is the ATP concentration corresponding to half of the maximum reaction rate, were determined.

Differential scanning calorimetry (DSC) measurements

DSC measurements were performed with a SETARAM Micro DSC-III calorimeter in the range of 20 to 100 °C at a heating rate of 0.3 $K \cdot min^{-1}$. The sample (wild type and D67N protein) and the reference (buffer) were equilibrated to ± 0.05 mg to avoid corrections for the heat capacity of the vessels.

A second recording of the denatured sample was measured to correct the baseline. The melting temperature (Tm) of the thermal decomposition curves was analysed using OriginLab Origin2021 software.

Fluorescence anisotropy-based nucleotide-binding assays

Fluorescence anisotropy is sensitive to the binding of ligands to proteins[4]. Changes in anisotropy are caused by changes in the mobility of the fluorophore. The addition of OaPAC to MANT-ATP increases the fluorescence anisotropy of N-methylantranilolyl (the fluorescent moiety of MANT-ATP), as the binding of MANT-ATP to OaPAC results in an increase in the rotational inertia of the candidate moiety and thus slows down its rotation.

Since the affinity of ATP in the dark or light state of the protein was not known, we measured the binding affinity (K_D) of a fluorescently labelled ATP analogue (MANT-ATP) for the wild-type and D67N mutant using a nucleotide binding assay based on fluorescence anisotropy measurements. These assays were performed at room temperature using 2 μM MANT-ATP. This is a hydrolysable, fluorescently labelled ATP with an emission at 450 nm upon excitation at 350 nm. Measurements were performed with a Fluorolog Jobin Yvon Horiba spectrofluorometer in the L format equipped with a polarization accessory. K_D values were determined by fitting the following quadratic binding equation:

$$\frac{r-r_A}{r_{AT}-r_A} = \frac{A_0+T_0+K_D-\sqrt{(A_0+T_0+K_D)^2-4\cdot A_0\cdot T_0}}{2},$$

where A_o and T_o are the total MANT-ATP/cAMP and OaPAC concentrations, r_A is the steady state anisotropy of MANT-ATP/cAMP in the absence of OaPAC, r_{AT} is the anisotropy of MANT-ATP/cAMP at saturating OaPAC levels and K_D is the dissociation constant of the MANT-ATP/cAMP-OaPAC complex, respectively.

Results

Transient absorption measurements

Transient absorption measurements were performed to characterise the primary photochemistry of the D67N mutant. The distinctly different absorption spectra of different redox states of the flavin chromophore can be used to spectrally model[2,3] the Evolution Associated Spectra (EAS) (OD(λ)) obtained from global analysis of the raw data to identify flavin and amino acid radicals detected at different delays after excitation. The transient absorption spectra measured for the D67N mutant of OaPAC are similar to those of other (oxidized) flavoproteins, including wild-type OaPAC[66,67]: around 450 nm, an intense negative peak (bleaching) is observed, which is associated with the disappearance of flavin $S_0 \rightarrow S_1$ absorption. The positive peak around 510 nm is attributed to the absorption of the excited state, while the broad ~550 nm peak observed at early time delays is attributed to the stimulated emission of flavin (Figure 4A).

For the global analysis, assuming a sequential scheme, the data were globally fitted with three different time constants (5 ps, 65 ps and infinity) (Figure 4B), similarly to measurements on the wild-type protein[33]. As for the wild-type protein, the time constant of the first EAS was found to be 5 ps and as a result EAS1 can be assigned to the difference spectrum of excited and oxidized flavin (FAD*-FADox). The EAS2 time constant of 65 ps for the D67N mutant suggests a faster phase compared to the wild-type (EAS2 = 83 ps). The 65 ps component was fitted as a linear combination of the ($FADH^{\bullet}$-FAD) and (FAD*-FADox) spectra, since fluorescence measurements show that the excited state is also present at the longer time constant. The $FADH^{\bullet}$ and FADox spectra were used to construct the ($FADH^{\bullet}$-FAD) spectrum and the 5-ps EAS was used to construct the (FAD*-FADox) spectrum. The shorter time constant measured for the mutant also indicates faster recombination of the radical pair.

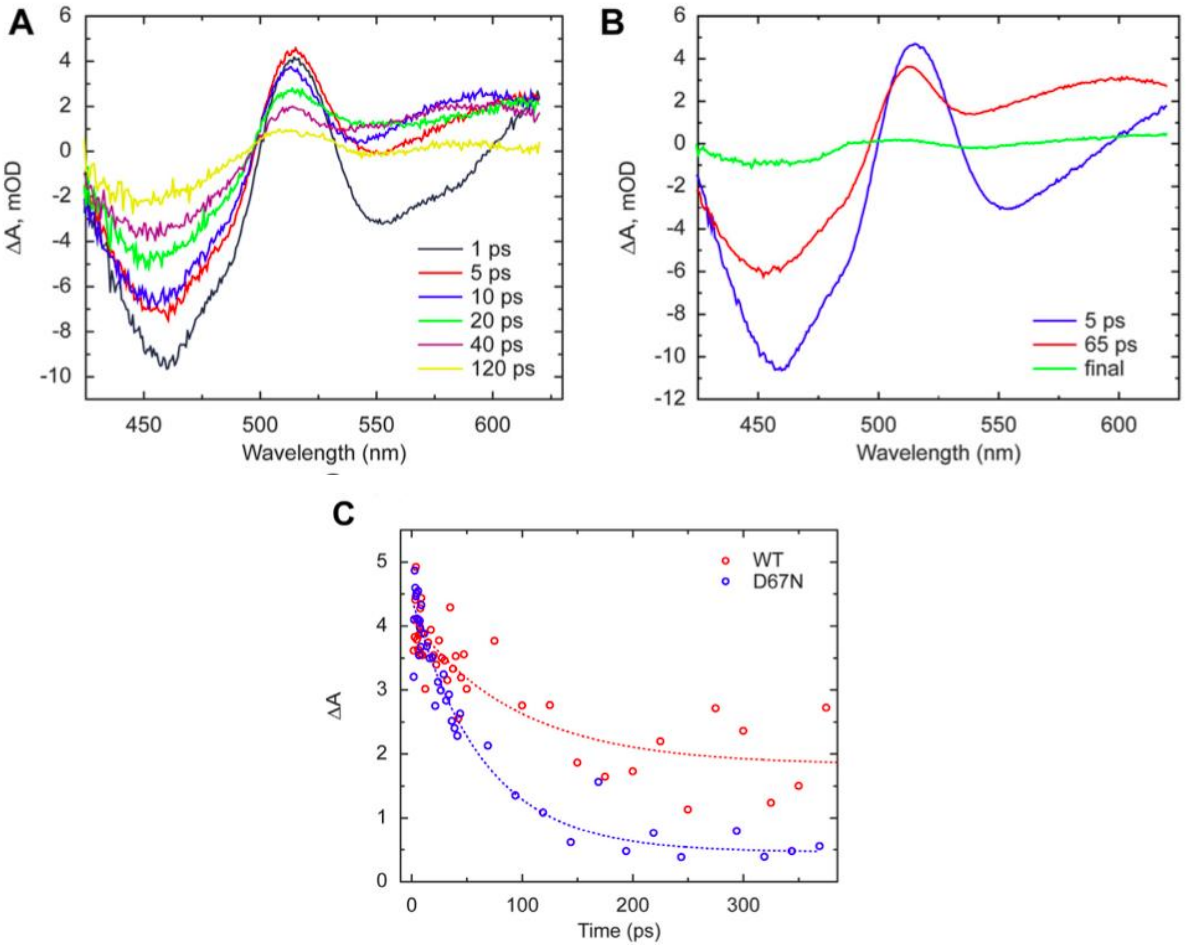

Figure 4. *A) Transient absorption measurements on the D67N mutant at different time delays B) EAS spectra obtained after global analysis C) Individual kinetics of wild-type and D67N OaPAC measured at 505 nm. Using monoexponential fitting, the time constants of wild type and D67N were 90 ± 30 ps and 64 ± 8 ps, respectively.*

The kinetics of relaxation of FAD* by electron and proton transfer to flavin are dispersive and the slower phases are kinetically inseparable from the kinetics of the formation of the $FADH^{\bullet}$ intermediate state. The final state indicates the red-shifted FADox state. From the time constants obtained, it follows that the neutral radical is formed within 5 ps after the excited state of FAD. Then, within 65 ps the FAD is oxidized. The faster relaxation of FAD* is indicated by the fact that the relative contribution of FAD* to EAS2 is smaller in D67N (~60%) than in the wild type (~75%). In addition to the faster phase of the D67N OaPAC, differences in the shape of EAS2 were also observed between the wild type and the mutant. At 505 nm, the kinetics of the flavin excited-state peak is spectacularly faster for D67N than for the wild-type protein (Figure 4 C). Using a monoexponential fit, the time constants of wild-type and D67N were 90 ± 30 ps and 64 ± 8 ps, respectively. The faster FAD* decrease confirms our hypothesis that the

replacement of aspartic acid with a neutral or positively charged residue accelerates the electron transfer process.

Fitting the specific kinetics to the absorption maxima of the excited state, we also observed a faster decay in D67N compared to the wild type, supporting the primary observation that the quenching of the excited state, probably due to electron transfer, is more efficient in the mutant. The time constants show that the excited state of FAD formed immediately after excitation relaxes to the next state within 5 ps, indicating the presence of a neutral flavin radical. The final state is a structure characteristic of the clear state of the FAD, which lasts longer than the window of the measurement:

$$\text{Blue light} \rightarrow \text{FAD}^* \rightarrow^{5\text{ps}} \rightarrow \text{FADH}^{\bullet} \rightarrow^{65\text{ps}} \rightarrow \text{FAD}_{\text{ox}}$$

Ultrafast transient fluorescence spectroscopy experiments

Ultrashort transient fluorescence measurements were performed on our home-built Kerr-gate setup with the intention to gain further insight into the effect of the D67N mutation on the electron transport. Figures 5A and B show the EAS spectra obtained by global fitting of the transient fluorescence data series. The fluorescence emission peak at ~513 nm is higher than the value observed for AppA (~500 nm) and significantly lower than that of the free flavin (~530 nm)[68]. The fluorescence emission wavelength indicates that flavin is hidden in a compact environment and there is no significant difference between the emission maxima of the wild-type and the mutant. This suggests that the mutation did not result in a significant change of the flavin environment. The decay of the fluorescence emission of wild-type OaPAC was found to be highly dispersive. Global splicing was described in both samples with three EAS components analogous to the TA experiments, with a faster time constant for D67N compared to WT. Thus, the transient fluorescence data series was well described with the same three lifetimes (5 ps, 83 ps and ∞ for the wild-type protein and 5 ps, 60 ps, and ∞ for the mutant) as in the TA experiments.

The corresponding EAS (assuming a sequential scheme (1→2→3)) spectra all have a maximum around 513 nm, suggesting that they are derived from protein-bound flavin. For a direct comparison between the decay of the fluorescence emission of wild-type and D67N, we compared the kinetics observed at 513 nm. From Figure 5C, it can be seen that the lifetime of the excited state relaxation in the D67N mutant is almost half (25 ± 2 ps) of that observed for the wild-type protein (40 ± 2 ps). This result clearly demonstrates that electron transfer is faster overall in the D67N OaPAC mutant. Yet, as shown above, this modestly faster initial electron transfer does not lead to a higher yield (quantum efficiency) of the signalling state, presumably due to strongly enhanced back PCET from $\text{FADH}^{\bullet}$ to the resting dark state.

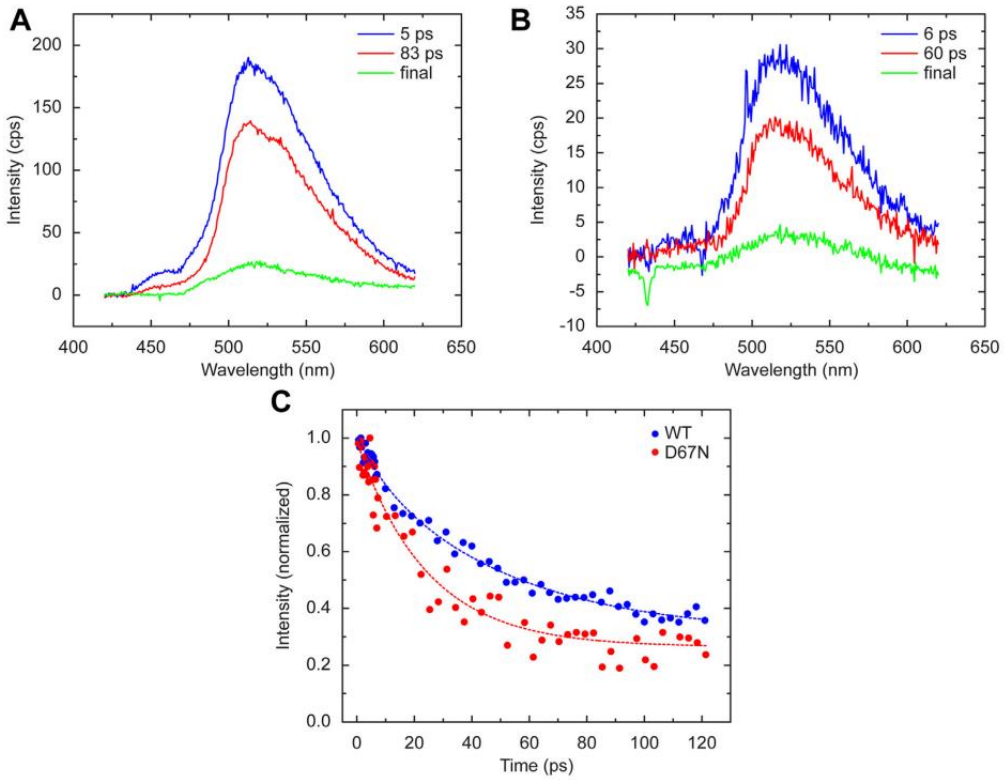

Figure 5. *A) EAS spectra obtained from global analysis of wild-type transient fluorescence data. The global fit result shows heterogeneous relaxation of flavin B) EAS spectra obtained by global analysis of transient fluorescence data from the D67N mutant C) Specific kinetics of fluorescence decay observed at 513 nm. Using a monoexponential fit, the average lifetime of the wild-type fluorescence relaxation was found to be 40 ± 2 ps and 25 ± 2 ps for D67N.*

Indirect measurement of cAMP

First, the adenylate cyclase activity of the wild-type OaPAC and D67N OaPAC was monitored over time using a spectrophotometric assay that indirectly detects the release of pyrophosphate by OaPAC (OD360) when it converts ATP to cAMP. Figure 6A shows the dark- and light-induced enzyme activities of 1 µM wild type OaPAC and 1 µM D67N mutant OaPAC in the presence of 500 µM ATP. In the dark, the enzyme activity was very low. Under illumination, the conversion rates strongly increased in the wild type and D67N mutant. The D67N mutant, however, converts ATP at a higher rate (more efficiently) than the wild type, making this mutant a starting point for optogenetic tuning of PACs. To determine kinetic constants, enzymatic assays were performed using increasing amounts of substrate (ATP). The results were evaluated using the classical Michaelis-Menten function (Figure 6B).

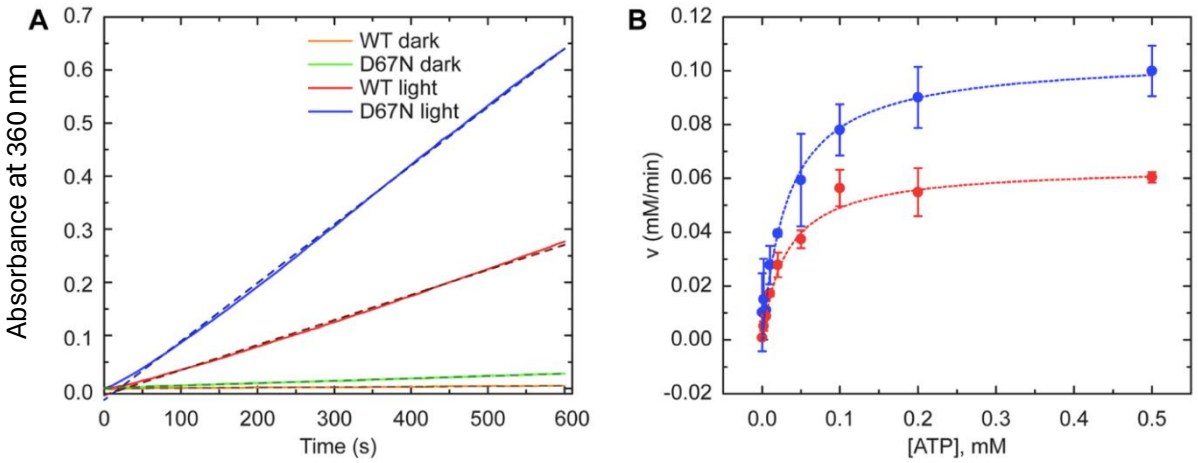

Figure 6. *A) Kinetics of ATP conversion in the dark- and light-adapted states of wild-type and D67N OaPAC. In the dark state, the rate of ATP conversion is slightly higher in the D67N mutant than in the wild type. In the light state in the presence of 0.5 mM ATP, the rate of conversion was higher in the mutant than in the wild type.*
B) Michaelis-Menten diagram of enzyme activity of wild type (lower) and D67N (upper), under illumination. v_{max} *is increased in the D67N mutant.*

These assays showed increased cAMP production in D67N OaPAC: the maximum conversion rate was 1.5-fold higher in the mutant (0.100 ± 0.002 mM/min) than in the wild type (0.064 ± 0.007 mM/min). The concentration of the half-maximal rate (K_M) was also slightly higher in the mutant than in the wild type, but more importantly, the catalytic constant (k_{cat}), which defines the number of substrate molecules that can be converted into product by each enzyme site per unit time, was ~1.5-fold higher in D67N (50.05 1/min) than in wild-type OaPAC (32.2 1/min).

Light to dark recovery experiments

Similar to other BLUF domain proteins, the absorption spectrum of the D67N mutant shows a typical red shift of the absorption peak (from 442 nm to 455 nm) after irradiation with blue light, which characterises the S_0-S_1 transition. To characterise the relationship between the photophysics of the BLUF domain and the functional dynamics of the mutant, we have also performed recovery experiments. The regeneration of the BLUF domain from the light to the dark state - the relaxation of the photoactivated state - can range from a few seconds to several tens of minutes; in OaPAC it is only a few seconds[33]. The regeneration of the D67N mutant and wild-type OaPAC was monitored by recording absorbance at 492 nm. The regeneration rate of the mutant is significantly lower than that of the wild-type OaPAC (Figure 7B).

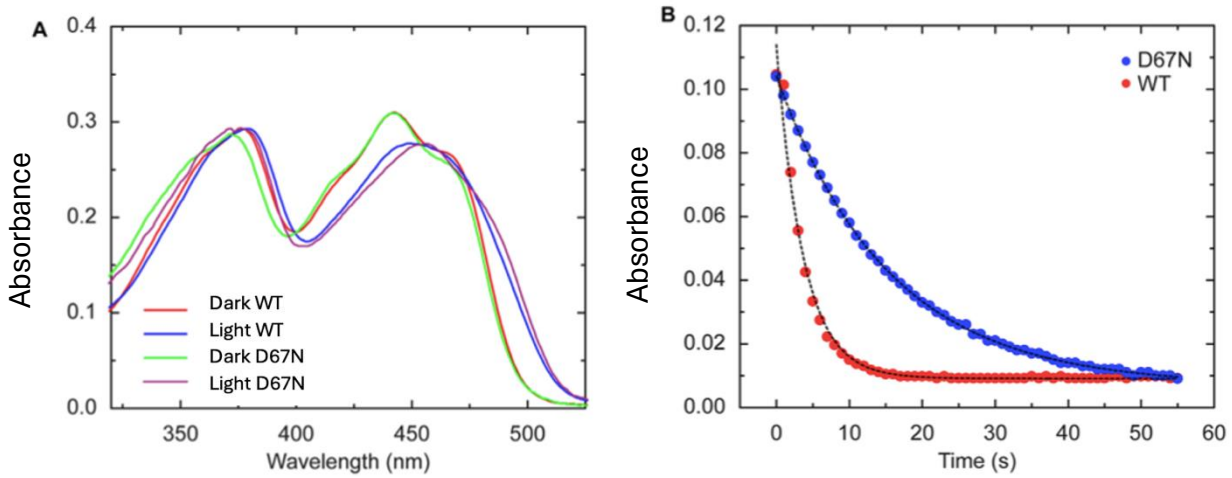

Figure 7. *A) Absorption spectra of wild-type and D67N OaPAC in the dark and light states B) Rate of return to the dark state of wild-type and D67N OaPAC by monitoring absorption at 490 nm. The wild-type OaPAC relaxes to the dark state in 3.6 s, for D67N this time is 15.3 s.*

Figure 7A. shows the dark and light absorption spectra of wild-type and D67N OaPAC, and Figure 7B shows the relaxation to dark state and recovery of wild-type and D67N OaPAC. Based on the absorption spectra, the absorptions of the wild type and the mutant are very similar in the dark state: the peak of the S_0-S_1 transition is the same for both proteins, with a maximum at 442 nm. In the mutant, a blue shift of the S_0-S_2 transition of 4 nm is observed (376 nm for the wild type and 372 nm for the mutant). In the light state, the S_0-S_1 peak is shifted to 452 nm in the WT and 456 nm in the mutant. The S_0-S_2 peak shifts from 376 nm to 379 nm in the WT and from 372 nm to 376 nm in the mutant. The slower regeneration of D67N suggests that the protein spends more time after light excitation in a structure that allows cAMP generation. Altogether, the mutant adopts a structure that is not only more favourable for ATP to cAMP conversion but also slows down the rearrangement to the original structure.

DSC measurements

The difference in enzymatic activity and the return to the dark state suggests that the introduced mutation has altered the protein structure. To gain insight into the origin of the increase in cAMP production, differential scanning calorimetry (DSC) experiments were performed on the wild-type and D67N OaPAC protein to investigate their thermostability. These measurements show significant differences between the mutant and wild-type OaPAC. The thermal denaturation of the wild type showed a steep endothermic unfolding with a Tm of 68.1°C and a ΔH of 0.078 J/g. Measurements of D67N resulted in a lower Tm (62.1°C) with a lower ΔH (0.069 J/g). The lower ΔH value of D67N and the Tm value lower by 6°C indicate that the thermodynamic stability of D67N OaPAC is significantly reduced by the mutation. This suggests a less compact and more flexible conformation of the D67N mutant, and thus a structural change. Based on the DSC measurements, we conclude that the increased enzyme

activity of D67N OaPAC is due to a more flexible structure, i.e. a more favourable structure, and not to differences observed in the electron transfer process.

Fluorescence anisotropy-based nucleotide-binding assays

Since the affinity of ATP in the dark or light state of the protein was not known, we measured the binding affinity (K_D) of a fluorescently labelled ATP analogue (MANT-ATP) in the wild type and D67N mutant using a nucleotide binding assay based on fluorescence anisotropy measurements. The 2 μM MANT-ATP was excited at 350 nm and fluorescence emission was detected at 450 nm with increasing OaPAC concentration in the range 0-98 μM. Since OaPAC excited at 350 nm emitted at >500 nm, flavin emission does not contribute to the anisotropy measurements. The affinity (K_D) of wild-type and D67N OaPAC for MANT-ATP was found to be 2.2 ± 0.4 mM and 7.7 ± 1.6 mM, respectively. Again, the lower affinity in the mutant suggests that the mutation induced a structural change, already seen in the DSC measurements, that affected the ATP binding affinity and the yield of cAMP production.

Summary, conclusions

In a series of experiments, we investigated the effect of the primary electron transfer process at the photosensory BLUF domain of OaPAC on the enzymatic activity of the protein. The AC activity of OaPAC was increased by optimising the electron transfer process in the BLUF domain: an aspartic acid was replaced by asparagine near the flavin chromophore by targeted mutagenesis. The specific mutant (D67N) was predicted to alter the kinetics of the electron transfer. Our ultrafast transient absorption and transient fluorescence measurements showed that the electron transfer rate in the mutant was significantly higher compared to the wild-type OaPAC. The significant increase in the rate of ATP-cAMP conversion resulted in higher enzyme activity: v_{max} was more than twofold and K_M was fourfold in the mutant. Enzymatic assays also showed that under blue light illumination, the mutant produced ~1.6 times more cAMP than wild-type OaPAC. Interestingly, the rate of return from the light state to the dark state was ~4-fold longer in the mutant than in wild-type OaPAC.

The faster electron transfer rate and the higher enzyme activity seem to be related to the protein structure: calorimetric and anisotropy measurements show that the mutant has a less compact and more flexible structure than the wild type. Our structural experiments suggest that the mutation induced a structural change, which may also affect enzymatic activity.

Our experiments on the D67N OaPAC mutant confirmed the hypothesis that the replacement of aspartic acid by asparagine accelerates the photoinduced electron transfer process and flavin oxidation. The mutation also led to an increase in cAMP conversion, the primary cause of which is probably not the differences observed in the electron transfer process but a change in the structure of the mutant.

Summary of our experimental procedures and their results with interpretation

Measurement procedure	**Name, symbol and unit of measured parameter**	**Measurement results**			
		Wild-type OaPAC	**D67N mutant**	**Change, trend**	**Interpretation**
Enzymatic activity measurement: cAMP yield measured by absorption spectrophotometry (pyrophosphate assay)	Maximum rate of transformation v_{max} [mM/perc]	0,064 ±0,007	0,1 ±0,002	↑~1,6×	Higher enzyme activity in the mutant
	Catalytic constant k_{cat}[1/min]	32,2	50,05	↑~1,6×	Mutant enzyme sites can convert more substrate molecules into products in a unit time
	Half maximum rate concentration K_M [mM]	0,031 ±0,001	0,041 ±0,005	↑~1,3×	Higher enzyme activity in the mutant
Time-dependent absorption spectrophotometry	Time to return to a dark state [s]	3,6	15,3	↑~4×	The mutant is in the light state for longer: it spends longer in the ATP-cAMP conversion structure
Ultrafast transient absorption spectroscopy	Excited state relaxation time [ps]	90±30	64±8	↓~0,7×	The electron transfer rate in the mutant was significantly higher compared to the wild-type OaPAC
Kerr-gated fluorescent spectroscopy	Fluorescent lifetime τ [ps]	40±2	25±2	↓~0,6×	
Differential scanning calorimetry	Melting temperature *T*m [°C]	68,1	62,1	↓-6°C	The mutant unfolds more easily and has a more flexible structure.
	Enthalpy change ΔH [J/g]	0,078	0,069	↓~0,9×	The mutant requires less energy to denature→ its structure is less compact than that of the WT
Steady-state fluorescence anisotropy	Binding affinity K_D [mM]	2,2±0,4	7,7±1,6	↑~3,5×	The mutation induced a structural change that affected ATP binding affinity and the yield of cAMP production.

Publications

Publications the thesis is based on

1) *Photocycle alteration and increased enzymatic activity in genetically modified photoactivated adenylate cyclase OaPAC*
Katalin Raics, Katalin Pirisi , Bo Zhuang , Zsuzsanna Fekete , Nikolett Kis-Bicskei, Ildiko Pecsi, Kinga Pozsonyi Ujfalusi, Elek Telek, Yin Li, Jinnette Tolentino Collado, Peter J. Tonge, Stephen R. Meech, Marten H. Vos, Emoke Bodis, and Andras Lukacs
J Biol Chem. 2023 Aug;299(8):105056. doi: 10.1016/j.jbc.2023.105056. IF: 5,5

2) *Fluorescence lifetime distributions report on protein destabilisation in quenching experiments*
Emőke Bódis, Katalin Raics, Miklós Nyitrai, Zsuzsa Majer, András Lukács
J Photochem Photobiol B. 2013 Dec 5;129:108-14. doi: 10.1016/j.jphotobiol.2013.10.004. IF:2,8

Further publications

3) *Functional dynamics of a single tryptophan residue in a BLUF protein revealed by fluorescence spectroscopy*
Kristof Karadi, Sofia Kapetanaki, Katalin Raics, Ildiko Pecsi, Robert Kapronczai, Zsuzsanna Fekete, James Iuliano, Jinnette Collado, Agnieszka Gil, Jozsef Orban, Miklos Nyitrai, Greg Greetham, Marten Vos, Peter Tonge, Stephen Meech, Andras Lukacs
Sci Rep. 2020 Feb 6;10(1):2061. doi: 10.1038/s41598-020-59073-5.

4) *Developmental changes in the expression level of connexin36 in the rat retina*
Tamás Kovács-Öller, Katalin Raics, József Orbán, Miklós Nyitrai, Béla Völgyi
Cell Tissue Res. 2014 Nov;358(2):289-302. doi: 10.1007/s00441-014-1967-9.

5) *The role of electron transfer in the enzymatic activity of a photoactivable adenylate cyclase*
Elek Telek, Katalin Raics, Katalin Pirisi, Robert Kapronczai, Emoke Bodis, Ildiko Pecsi, Marten Vos, Bo Zhuang, Andras Lukacs
Biophysical Journal, vol. 122, issue 3, p. 43

6) *Position of W104 in AppA BLUF domain revealed by fluorescence spectroscopy*
K. Raics, K. Pirisi, J. Orban, R. Brust, G. Greg, T. Mike, T. Pete, M. Stephen
9th European-Biophysical-Societies-Association Congress

Bibliography

1 Kao, Y. *et al.* Ultrafast dynamics of flavins in five redox states. *Journal of the American Chemical Society* **130**, 13132-13139 (2008). https://doi.org/10.1021/ja8045469

2 Snellenburg, J., Laptenok, S., Seger, R., Mullen, K. & van Stokkum, I. Glotaran: A Java-Based Graphical User Interface for the R Package TIMP. *Journal of Statistical Software* **49**, 1-22 (2012). https://doi.org/10.18637/jss.v049.i03

3 van Stokkum, I. H., Larsen, D. S. & van Grondelle, R. Global and target analysis of time-resolved spectra. *Biochim Biophys Acta* **1657**, 82-104 (2004). https://doi.org/10.1016/j.bbabio.2004.04.011

4 Lakowicz, J. R. *Principles of fluorescence spectroscopy*. (Springer, 2006).

5 Laptenok, S. P., Nuernberger, P., Lukacs, A. & Vos, M. H. Subpicosecond Kerr-gate spectrofluorometry. *Methods Mol Biol* **1076**, 321-336 (2014). https://doi.org/10.1007/978-1-62703-649-8_13

6 Sancar, A. Structure and function of DNA photolyase and cryptochrome blue-light photoreceptors. *Chem Rev* **103**, 2203-2237 (2003). https://doi.org/10.1021/cr0204348

7 Brettel, K. & Vos, M. H. Spectroscopic resolution of the picosecond reduction kinetics of the secondary electron acceptor A1 in photosystem I. *FEBS Lett* **447**, 315-317 (1999). https://doi.org/10.1016/s0014-5793(99)00317-8

8 Aubert, C., Vos, M. H., Mathis, P., Eker, A. P. & Brettel, K. Intraprotein radical transfer during photoactivation of DNA photolyase. *Nature* **405**, 586-590 (2000). https://doi.org/10.1038/35014644

9 Byrdin, M., Eker, A., Vos, M. & Brettel, K. Dissection of the triple tryptophan electron transfer chain in Escherichial coli DNA photolyase: Trp382 is the primary donor in photoactivation. *Proceedings of the National Academy of Sciences of the United States of America* **100**, 8676-8681 (2003). https://doi.org/10.1073/pnas.1531645100

10 Lukacs, A. *et al.* Role of the middle residue in the triple tryptophan electron transfer chain of DNA photolyase: Ultrafast spectroscopy of a Trp -> Phe mutant. *Journal of Physical Chemistry B* **110**, 15654-15658 (2006). https://doi.org/10.1021/jp063686b

11 Lukacs, A., Eker, A., Byrdin, M., Brettel, K. & Vos, M. Electron Hopping through the 15 angstrom Triple Tryptophan Molecular Wire in DNA Photolyase Occurs within 30 ps. *Journal of the American Chemical Society* **130**, 14394-+ (2008). https://doi.org/10.1021/ja805261m

12 Byrdin, M. *et al.* Quantum Yield Measurements of Short-Lived Photoactivation Intermediates in DNA Photolyase: Toward a Detailed Understanding of the Triple Tryptophan Electron Transfer Chain. *Journal of Physical Chemistry a* **114**, 3207-3214 (2010). https://doi.org/10.1021/jp9093589

13 Lukacs, A. *et al.* Photoexcitation of the blue light using FAD photoreceptor AppA results in ultrafast changes to the protein matrix. *J Am Chem Soc* **133**, 16893-16900 (2011). https://doi.org/10.1021/ja2060098

14 Brust, R. *et al.* Proteins in action: femtosecond to millisecond structural dynamics of a photoactive flavoprotein. *J Am Chem Soc* **135**, 16168-16174 (2013). https://doi.org/10.1021/ja407265p

15 Lukacs, A., Tonge, P. J. & Meech, S. R. Photophysics of the Blue Light Using Flavin Domain. *Acc Chem Res* **55**, 402-414 (2022). https://doi.org/10.1021/acs.accounts.1c00659

16 Li, G., Sichula, V. & Glusac, K. D. Role of adenine in thymine-dimer repair by reduced flavin-adenine dinucleotide. *J Phys Chem B* **112**, 10758-10764 (2008). https://doi.org/10.1021/jp804506t

17 van den Berg, P. A., van Hoek, A., Walentas, C. D., Perham, R. N. & Visser, A. J. Flavin fluorescence dynamics and photoinduced electron transfer in Escherichia coli glutathione reductase. *Biophys J* **74**, 2046-2058 (1998). https://doi.org/10.1016/S0006-3495(98)77911-1

18 van den Berg, P. A. *et al.* Exploring the conformational equilibrium of E. coli thioredoxin reductase: characterization of two catalytically important states by ultrafast flavin fluorescence spectroscopy. *Protein Sci* **10**, 2037-2049 (2001). https://doi.org/10.1110/ps.06701

19 van den Berg, P. A., Widengren, J., Hink, M. A., Rigler, R. & Visser, A. J. Fluorescence correlation spectroscopy of flavins and flavoenzymes: photochemical and photophysical aspects. *Spectrochim Acta A Mol Biomol Spectrosc* **57**, 2135-2144 (2001). https://doi.org/10.1016/s1386-1425(01)00494-2

20 Bonetti, C. *et al.* The light activation mechanism of a novel blue-light photoreceptor. *Biophysical Journal*, 337A-337A (2007).

21 Gauden, M. *et al.* Photocycle of the flavin-binding photoreceptor AppA, a bacterial transcriptional antirepressor of photosynthesis genes. *Biochemistry* **44**, 3653-3662 (2005). https://doi.org/10.1021/bi047359a

22 Kennis, J. *et al.* The LOV2 domain of phototropin: A reversible photochromic switch. *Journal of the American Chemical Society* **126**, 4512-4513 (2004). https://doi.org/10.1021/ja031840r

23 Kennis, J. T. & Groot, M. L. Ultrafast spectroscopy of biological photoreceptors. *Curr Opin Struct Biol* **17**, 623-630 (2007). https://doi.org/10.1016/j.sbi.2007.09.006

24 Laan, W. *et al.* On the mechanism of activation of the BLUF domain of AppA. *Biochemistry* **45**, 51-60 (2006). https://doi.org/10.1021/bi051367p

25 Masuda, S., Hasegawa, K. & Ono, T. A. Light-induced structural changes of apoprotein and chromophore in the sensor of blue light using FAD (BLUF) domain of AppA for a signaling state. *Biochemistry* **44**, 1215-1224 (2005). https://doi.org/10.1021/bi047876t

26 Brust, R. *et al.* Ultrafast Structural Dynamics of BlsA, a Photoreceptor from the Pathogenic Bacterium. *J Phys Chem Lett* **5**, 220-224 (2014). https://doi.org/10.1021/jz4023738

27 Ohki, M. *et al.* Structural insight into photoactivation of an adenylate cyclase from a photosynthetic cyanobacterium. *PNAS* **113**, 6659-6664 (2016). https://doi.org/10.1073/pnas.1517520113

28 Ohki, M. *et al.* Molecular mechanism of photoactivation of a light-regulated adenylate cyclase. *Proceedings of the National Academy of Sciences of the United States of America* **114**, 8562-8567 (2017). https://doi.org/10.1073/pnas.1704391114

29 Nagahama, T., Suzuki, T., Yoshikawa, S. & Iseki, M. Functional transplant of photoactivated adenylyl cyclase into Aplysia mechanosensory neurons. *Neuroscience Research* **58**, S241-S241 (2007). https://doi.org/10.1016/j.neures.2007.06.593

30 Jansen, V. *et al.* Controlling fertilization and cAMP signaling in sperm by optogenetics. *Elife* **4** (2015). https://doi.org/10.7554/eLife.05161

31 Ohki, M. *et al.* Structural insight into photoactivation of an adenylate cyclase from a photosynthetic cyanobacterium. *Proceedings of the National Academy of Sciences of the United States of America* **113**, 6659-6664 (2016). https://doi.org/10.1073/pnas.1517520113

32 Ohki, M. *et al.* Structural basis for photoactivation of a light-regulated adenylate cyclase from the photosynthetic cyanobacterium Oscillatoria acuminata. *Acta Crystallographica a-Foundation and Advances* **72**, S251-S251 (2016). https://doi.org/10.1107/S2053273316096194

33 Collado, J. *et al.* Unraveling the Photoactivation Mechanism of a Light-Activated Adenylyl Cyclase Using Ultrafast Spectroscopy Coupled with Unnatural Amino Acid Mutagenesis. *Acs Chemical Biology* **17**, 2643-2654 (2022). https://doi.org/10.1021/acschembio.2c00575

34 Lukacs, A. *et al.* BLUF domain function does not require a metastable radical intermediate state. *J Am Chem Soc* **136**, 4605-4615 (2014). https://doi.org/10.1021/ja4121082

35 Mathes, T., van Stokkum, I., Bonetti, C., Hegemann, P. & Kennis, J. The Hydrogen-Bond Switch Reaction of the Blrb Bluf Domain of Rhodobacter sphaeroides. *Journal of Physical Chemistry B* **115**, 7963-7971 (2011). https://doi.org/10.1021/jp201296m

36 Zirak, P. *et al.* Photodynamics of the small BLUF protein BlrB from Rhodobacter sphaeroides. *J Photochem Photobiol B* **83**, 180-194 (2006). https://doi.org/10.1016/j.jphotobiol.2005.12.015

37 Bonetti, C. *et al.* The Role of Key Amino Acids in the Photoactivation Pathway of the Synechocystis Slr1694 BLUF Domain. *Biochemistry* **48**, 11458-11469 (2009). https://doi.org/10.1021/bi901196x

38 Gil, A. A. *et al.* Photoactivation of the BLUF Protein PixD Probed by the Site-Specific Incorporation of Fluorotyrosine Residues. *J Am Chem Soc* **139**, 14638-14648 (2017). https://doi.org/10.1021/jacs.7b07849

39 Fujisawa, T., Takeuchi, S., Masuda, S. & Tahara, T. Signaling-State Formation Mechanism of a BLUF Protein PapB from the Purple Bacterium Rhodopseudomonas palustris Studied by Femtosecond Time-Resolved Absorption Spectroscopy. *J Phys Chem B* **118**, 14761-14773 (2014). https://doi.org/10.1021/jp5076252

40 Goings, J. & Hammes-Schiffer, S. Early Photocycle of Slr1694 Blue-Light Using Flavin Photoreceptor Unraveled through Adiabatic Excited-State Quantum Mechanical/Molecular Mechanical Dynamics. *Journal of the American Chemical Society* **141**, 20470-20479 (2019). https://doi.org/10.1021/jacs.9b11196

41 Mátyus, L., Szöllosi, J. & Jenei, A. Steady-state fluorescence quenching applications for studying protein structure and dynamics. *J Photochem Photobiol B* **83**, 223-236 (2006). https://doi.org/10.1016/j.jphotobiol.2005.12.017

42 Eftink, M. R. & Ghiron, C. A. Dynamics of a protein matrix revealed by fluorescence quenching. *Proc Natl Acad Sci U S A* **72**, 3290-3294 (1975). https://doi.org/10.1073/pnas.72.9.3290

43 Gratton, E., Jameson, D. M., Weber, G. & Alpert, B. A model of dynamic quenching of fluorescence in globular proteins. *Biophys J* **45**, 789-794 (1984). https://doi.org/10.1016/S0006-3495(84)84223-X

44 Somogyi, B. *et al.* A double-quenching method for studying protein dynamics: separation of the fluorescence quenching parameters characteristic of solvent-exposed and solvent-masked fluorophors. *Biochemistry* **24**, 6674-6679 (1985). https://doi.org/10.1021/bi00344a056

45 Calhoun, D. B., Vanderkooi, J. M., Holtom, G. R. & Englander, S. W. Protein fluorescence quenching by small molecules: protein penetration versus solvent exposure. *Proteins* **1**, 109-115 (1986). https://doi.org/10.1002/prot.340010202

46 Tanaka, F. & Mataga, N. Fluorescence quenching dynamics of tryptophan in proteins. Effect of internal rotation under potential barrier. *Biophys J* **51**, 487-495 (1987). https://doi.org/10.1016/S0006-3495(87)83370-2

47 Somogyi, B. & Lakos, Z. Protein dynamics and fluorescence quenching. *J Photochem Photobiol B* **18**, 3-16 (1993). https://doi.org/10.1016/1011-1344(93)80035-8

48 Hild, G., Nyitrai, M., Gharavi, R., Somogyi, B. & Belágyi, J. Fluorescence quenching of the tryptophan emission from the F- and G-forms of actin. *J Photochem Photobiol B* **35**, 175-179 (1996). https://doi.org/10.1016/s1011-1344(96)07319-8

49 Clark, P. L., Liu, Z. P., Zhang, J. & Gierasch, L. M. Intrinsic tryptophans of CRABPI as probes of structure and folding. *Protein Sci* **5**, 1108-1117 (1996). https://doi.org/10.1002/pro.5560050613

50 Wang, W. Q., Xu, Q., Shan, Y. F. & Xu, G. J. Probing local conformational changes during equilibrium unfolding of firefly luciferase: fluorescence and circular dichroism studies of single tryptophan mutants. *Biochem Biophys Res Commun* **282**, 28-33 (2001). https://doi.org/10.1006/bbrc.2001.4539

51 Shirley, B. A. Urea and guanidine hydrochloride denaturation curves. *Methods Mol Biol* **40**, 177-190 (1995). https://doi.org/10.1385/0-89603-301-5:177

52 Pace, C. N. Determination and analysis of urea and guanidine hydrochloride denaturation curves. *Methods Enzymol* **131**, 266-280 (1986). https://doi.org/10.1016/0076-6879(86)31045-0

53 Eftink, M. R. & Ghiron, C. A. Does the fluorescence quencher acrylamide bind to proteins? *Biochim Biophys Acta* **916**, 343-349 (1987). https://doi.org/10.1016/0167-4838(87)90179-8

54 Carrington, C. D., Lapadula, D. M., Dulak, L., Friedman, M. & Abou-Donia, M. B. In vivo binding of [(14)C]acrylamide to proteins in the mouse nervous system. *Neurochem Int* **18**, 191-197 (1991). https://doi.org/10.1016/0197-0186(91)90185-g

55 Punyiczki, M. & Rosenberg, A. The effect of viscosity on the accessibility of the single tryptophan in human serum albumin. *Biophys Chem* **42**, 93-100 (1992). https://doi.org/10.1016/0301-4622(92)80011-s

56 Somogyi, B. *et al.* Coupling between external viscosity and the intramolecular dynamics of ribonuclease T1: a two-phase model for the quenching of protein fluorescence. *Biochim Biophys Acta* **1209**, 61-68 (1994). https://doi.org/10.1016/0167-4838(94)90137-6

57 Stein, D. L. A model of protein conformational substates. *Proc Natl Acad Sci U S A* **82**, 3670-3672 (1985). https://doi.org/10.1073/pnas.82.11.3670

58 Frauenfelder, H., Parak, F. & Young, R. D. Conformational substates in proteins. *Annu Rev Biophys Biophys Chem* **17**, 451-479 (1988). https://doi.org/10.1146/annurev.bb.17.060188.002315

59 Hong, M. K. *et al.* Conformational substates and motions in myoglobin. External influences on structure and dynamics. *Biophys J* **58**, 429-436 (1990). https://doi.org/10.1016/S0006-3495(90)82388-2

60 Alcala, J. R., Gratton, E. & Prendergast, F. G. Fluorescence lifetime distributions in proteins. *Biophys J* **51**, 597-604 (1987). https://doi.org/10.1016/S0006-3495(87)83384-2

61 Alcala, J. R., Gratton, E. & Prendergast, F. G. Interpretation of fluorescence decays in proteins using continuous lifetime distributions. *Biophys J* **51**, 925-936 (1987). https://doi.org/10.1016/S0006-3495(87)83420-3

62 Alcala, J. R., Gratton, E. & Prendergast, F. G. Resolvability of fluorescence lifetime distributions using phase fluorometry. *Biophys J* **51**, 587-596 (1987). https://doi.org/10.1016/S0006-3495(87)83383-0

63 Fiorini, R., Valentino, M., Wang, S., Glaser, M. & Gratton, E. Fluorescence lifetime distributions of 1,6-diphenyl-1,3,5-hexatriene in phospholipid vesicles. *Biochemistry* **26**, 3864-3870 (1987). https://doi.org/10.1021/bi00387a019

64 Fiorini, R. M., Valentino, M., Glaser, M., Gratton, E. & Curatola, G. Fluorescence lifetime distributions of 1,6-diphenyl-1,3,5-hexatriene reveal the effect of cholesterol on the microheterogeneity of erythrocyte membrane. *Biochim Biophys Acta* **939**, 485-492 (1988). https://doi.org/10.1016/0005-2736(88)90095-8

65 Laptenok, S. P. *et al.* A general approach for detecting folding intermediates from steady-state and time-resolved fluorescence of single-tryptophan-containing proteins. *Biochemistry* **50**, 3441-3450 (2011). https://doi.org/10.1021/bi101965d

66 Nag, L., Sournia, P., Myllykallio, H., Liebl, U. & Vos, M. Identification of the TyrOH(center dot+) Radical Cation in the Flavoenzyme TrmFO. *Journal of the American Chemical Society* **139**, 11500-11505 (2017). https://doi.org/10.1021/jacs.7b04586

67 Nag, L., Lukacs, A. & Vos, M. H. Short-Lived Radical Intermediates in the Photochemistry of Glucose Oxidase. *Chemphyschem* **20**, 1793-1798 (2019). https://doi.org/10.1002/cphc.201900329

68 Karadi, K. *et al.* Functional dynamics of a single tryptophan residue in a BLUF protein revealed by fluorescence spectroscopy. *Sci Rep* **10**, 2061 (2020). https://doi.org/10.1038/s41598-020-59073-5

69 Gil, A. *et al.* Mechanism of the AppABLUF Photocycle Probed by Site-Specific Incorporation of Fluorotyrosine Residues: Effect of the Y21 pKa on the Forward and Reverse Ground-State Reactions. *J Am Chem Soc* **138**, 926-935 (2016). https://doi.org/10.1021/jacs.5b11115